

Electronic properties of topological insulator candidate CaAgAs

Jayita Nayak¹, Nitesh Kumar¹, Shu-Chun Wu¹, Chandra Shekhar¹, Jörg Fink^{1,2},
Emile E.D. Rienks^{2,3}, Gerhard H. Fecher¹, Yan Sun¹ and Claudia Felser¹

¹Max Planck Institute for Chemical Physics of Solids, Nöthnitzer Str. 40, D-01187 Dresden, Germany.

²Leibniz Institut für Festkörper- und Werkstoffforschung IFW Dresden, D-01171 Dresden, Germany.

³Institute of Solid State Physics, Dresden University of Technology, Zellescher Weg 16, 01062 Dresden, Germany.

Abstract:

The topological phases of matter provide the opportunity to observe many exotic properties, like the existence of two dimensional topological surface states in the form of Dirac cone in topological insulators, chiral transport through open Fermi arc in Weyl semimetals etc. However, these properties can only affect the transport characteristics and therefore can be useful for applications only if the topological phenomena occur near the Fermi level. CaAgAs is a promising candidate, wherein the *ab-initio* calculations predict line-node at the Fermi level which on including spin-orbit coupling transforms into a topological insulator. In this report, we study the electronic structure of CaAgAs with angle resolved photoemission spectroscopy (ARPES), *ab-initio* calculations and transport measurements. The ARPES results show that the bulk valence band crosses the Fermi energy at Γ -point and the band dispersion matches the *ab-initio* calculations closely on shifting the Fermi energy by -0.5 eV. ARPES results are in good agreement with our transport measurements which show abundant p-type carriers.

The experimental realization of topological insulating (TI) phase, i. e. insulating in the bulk and symmetry protected electronic states at the surface, led to the explosion of current research activities.[1,2] Unremitting search for new topological states of matter has emerged as an active research field in condensed matter physics. Followed by the discovery of topological insulators, many new semimetallic/metallic phases have been proposed and investigated experimentally which host non-trivial band topology with vanishing densities of states near the Fermi level.[3-10] In general, the topological semimetals are classified into two major classes depending on whether conduction and valence bands coincide at a point or along a line in the three dimensional (3D) momentum space, leading to Dirac/Weyl semimetals or nodal line semimetals respectively. Band touching points in the topological semimetals are also protected by certain symmetries, analogous to TIs and thus are robust against external perturbations. 3D Dirac semimetals are experimentally realized in Na_3Bi [11,12] and Cd_2As_3 [9,13] compounds, which respect time reversal and inversion symmetry. On the other hand, violation of either inversion or time reversal symmetry in Dirac semimetals leads to the evolution of Weyl semimetals which have been verified experimentally in transition metal monophosphides.[8,14,15] Very recently, many topological nodal line semimetals have been predicted theoretically and only a few of them are experimentally confirmed by ARPES measurements. Among them, ZrSiS [15] and Cu_3PdN [16] are protected by inversion and time reversal symmetry and thus referred to as ‘Dirac nodal line’ whereas noncentrosymmetric PbTaSe_2 [10] which respects mirror reflection symmetry referred to as ‘Weyl nodal line’ semimetal.

Theoretical calculations usher the fact that the nodal line contacts are very fragile against spin-orbit coupling (SOC) [16,17] and the inclusion of SOC sometimes creates a gap at the band touching points of the nodal line, which drives the system into topological insulator or Weyl semimetal phase. Consequently, first principles calculations by Zeng *et al.* demonstrated the electronic structure of rare earth mononictides LaX ($\text{X} = \text{N}, \text{P}, \text{As}, \text{Sb}, \text{Bi}$).[18] Among them, LaN hosts ‘linked nodal rings’ when small SOC on nitrogen orbitals is neglected, but turning on SOC gaps the nodal rings at all except two points, which remain gapless enforcing the system to reside in Dirac semimetallic state.[18] Unlike LaN , compounds with other elements in the pnictogen group are found to be TIs due to strong SOC which was verified experimentally in LaBi compound.[19]

First principles calculations by Yamakage *et al.*, reveals that noncentrosymmetric compound, CaAgAs might host topological nodal line semimetal (NLS) state at the Fermi

energy in the absence of SOC[20] which on incorporating SOC, transforms into a TI wherein the Fermi level resides within the inverted band gap **Error! Bookmark not defined.** We study the electronic structure of CaAgAs by ARPES, *ab-initio* calculations and transport measurements and establish that the Fermi level is dominated by the bulk valence band because of the self-doping in the single crystals.

CaAgAs single crystals were grown in the bismuth flux. Ca, Ag, As and Bi pieces were weighed according to the composition $(\text{CaAgAs})_{0.1}\text{Bi}_{0.9}$ and transferred to an alumina crucible. It was then vacuum sealed inside a quartz tube. The content was heated to 1100 °C and kept at this temperature for 24 h. Then it was slowly cooled at a speed of 1.5 °C/h to 700 °C. At this temperature the flux was decanted off to obtain single crystals of CaAgAs. Crystal quality was confirmed by x-ray diffraction (XRD) and the composition was determined by energy dispersive analysis of x-rays (EDAX). The ARPES measurements were carried out at the UE112-PGM2b beamline in BESSY (Berlin) synchrotron using the 1³-ARPES end station that is equipped with a Scienta R4000 energy analyser. All measurements were performed at a temperature of 1 K at low photon energies ranging from 55-80 eV. Sample was cleaved in-situ at low temperature (~30 K). The total energy resolution was approximately 10 meV and the angular resolution was 0.2°.

The band structures are calculated by density-functional theory (DFT) with the projected augmented wave (PAW) potential implemented in the Vienna *ab initio* simulation package (VASP).[21,22] The generalized gradient approximation (GGA) [23] is used for the exchange-correlation energy. The surface electronic states are investigated by the tight-binding models, which is constructing by the maximally localized Wannier functions [24] for Ag-*s,d*, As-*p* and Ca-*d* orbitals.

Noncentrosymmetric Hexagonal pnictide CaAgAs crystallizes in ZrNiAl-type structure which belongs to the space group $P\bar{6}2m$ (No. 189) and the crystal structure is presented in Fig. 1(a). The important aspect for this space group resides in the fact that it retains mirror reflection symmetry but violates space inversion symmetry. Bulk Brillouin zone and high symmetry directions are marked in Fig. 1(b). Two dimensional projection of (0001) surface Brillouin zones are also depicted in Fig. 1(b). We have calculated bulk band structure of CaAgAs along Γ -M-K- Γ -A-L-H-A direction without considering spin-orbit coupling (SOC) (Fig. 1(c)). Since the crystal structure respects mirror reflection symmetry and breaks space inversion, calculations result in the appearance of nodal line semimetallic phase in CaAgAs in the absence of SOC. In the bulk calculations, we find that the line node is centred on Γ for both Γ M and Γ K directions. p_z orbital of As atoms contribute mainly in the

conduction band near Γ , whereas p_x, p_y orbitals of As along with s orbital of Ag constitute the valence band. Thus, the band inversion occurs between p_x, p_y and p_z orbitals of As. Now, if we turn on SOC as depicted in Fig. 1(d), due to the strong spin-orbit coupling of As atoms line nodes are gapped both along ΓM and ΓK directions and drives the system to TI phase. The evolution of Wannier centers are used to identify the topological order[25,26], which indicated a non-trivial topology and is consistent with previous work.[20] Further, we confirmed the TI phase by the direct surface state calculations with Green's function on the (0001) surface of CaAgAs termination. The Dirac point is 0.1 eV below the charge neutral point, which is still inside the inverted band gap.

We have performed ARPES measurement of CaAgAs (0001) surface. In order to characterise the surface we have performed core level photoemission measurement (Fig. 2(a)). We identify Ca $3p$ peak at 24 eV binding energy. As $3d$ peak appears at 39.48 eV and shows a spin-orbit splitting of 0.6 eV. Ag $4p$ peak (shown in the inset of Fig. 2(a)) intensity is strongly suppressed due to the cross-sectional effect. Absence of any impurity peak and the appearance of sharp Ca and As peaks in the corelevel spectra ensure the high quality of our crystal used for spectroscopic investigation. Fig. 2(b) demonstrates the Fermi surface of CaAgAs measured with 85 eV excitation energy and represents circular hole pocket centered at Γ . Red dotted line indicates the hexagonal Brillouin zone of CaAgAs. Constant energy surface at -0.35 eV is shown in Fig. 2(c) and reveals that the increase of binding energy results in the increase of the radius of hole pocket and starts merging with other $\bar{\Gamma}$ point. By down shifting the energy by 0.5 eV from the charge neutral point (Fig. 2(d)) well reproduces the experimental data. This is probably caused by small self-doping in our crystals. Both the experimental results and theoretical calculations demonstrate that the Dirac point is quite above E_F and thus the sample represents predominantly p -type behaviour which is consistent with our transport measurements which we discuss later. In order to access the Dirac point we have deposited Caesium but unfortunately, we could not shift the Fermi level. We have measured band dispersion along $\bar{M} - \bar{\Gamma} - \bar{M}$ direction (shown in Fig. 2(e)) and indicate the appearance of another hole like band below -0.2 eV within the outer hole like band. This inner band was not clearly resolved in the constant energy surface at -0.35 eV due to the overlapping with the outer band. Our theoretical calculations (Fig. 2 (f)) is in agreement with the experimental results. The band dispersion (Fig. 2(g)) along $\bar{K} - \bar{\Gamma} - \bar{K}$ is also consistent with the theoretical calculation (Fig. 2(h)).

We have performed photon energy dependent ARPES measurements in a wide photon energy range between 60 to 93 eV along $\bar{M} - \bar{\Gamma} - \bar{M}$ direction as illustrated in Fig. 3. We find that both the inner and outer hole pockets centered at $\bar{\Gamma}$ change significantly with the change of photon energy which indicates that the hole pockets results from the bulk bands since bulk bands are expected to disperse strongly with photon energy. Our theoretical calculations also confirm the bulk band character of the hole pocket.

The transport properties of CaAgAs are in good agreement with the ARPES data. The electrical resistivity at 2 K is $7.4 \times 10^{-5} \Omega\text{cm}$, which decreases with decreasing temperature and saturates at low temperature, typical of a metal (Fig 4(a)). This is in contrast to the topological insulators where the inverted gap lies at the Fermi level and resistivity increases on decreasing temperature with a plateau at low temperature due to the topological surface states. Magnetic field dependent Hall resistivity $\rho_{yx}(B)$ shows the existence of the hole-type charge carriers from its positive slope as shown in Fig. 4(b). This is expected for the valence band crossing the Fermi energy as proved earlier by ARPES. The behavior is very robust against temperature and there is a little change up to 300 K. We extracted the hole carrier concentration and mobility from the slope of $\rho_{yx}(B)$; at 2 K, the values are $1.67 \times 10^{20} \text{cm}^{-3}$ and $505 \text{cm}^2/\text{Vs}$. The carrier concentration is nearly independent of temperature indicating that the shape and the size of the Fermi surface remain intact. Under the framework of Drude model, considering spherical hole Fermi surface, the carrier concentration gives a Fermi wave vector of 0.17\AA^{-1} which is in close agreement with that observed in ARPES.

In summary, we studied the electronic properties of CaAgAs by employing ARPES, *ab-initio* calculations and transport. We establish that the bands at the Fermi level have bulk character. The agreement between ARPES and *ab-initio* calculations show that Dirac point is about 0.4 eV above the Fermi energy. Dominating hole-type carriers from the Hall resistivity data further support our claim.

References:

- [1] M. Z. Hasan, and C. L. Kane, *Rev. Mod. Phys.* **82**, 3045, (2010).
- [2] X.-L. Qi, and S.-C. Zhang, *Rev. Mod. Phys.* **83**, 1057, (2011).
- [3] X. Wan, A. M. Turner, A. Vishwanath, and S. Y. Savrasov, *Phys. Rev. B* **83**, 205101, (2011).
- [4] Z. Wang, Y. Sun, X.-Q. Chen, C. Franchini, G. Xu, H. Weng, X. Dai, and Z. Fang, *Phys. Rev. B* **85**, 195320, (2012).
- [5] H. Weng, C. Fang, Z. Fang, B. A. Bernevig, and X. Dai, *Phys. Rev. X* **5**, 011029, (2015).
- [6] Z. Wang, H. Weng, Q. Wu, X. Dai, and Z. Fang, *Phys. Rev. B* **88**, 125427, (2013).
- [7] A. A. Burkov, M. D. Hook, and L. Balents, *Phys. Rev. B* **84**, 235126, (2011).
- [8] S.-Y. Xu, I. Belopolski, N. Alidoust, M. Neupane, G. Bian, C. Zhang, R. Sankar, G. Chang, Z. Yuan, C.-C. Lee, S.-M. Huang, H. Zheng, J. Ma, D. S. Sanchez, B. Wang, A. Bansil, F. Chou, P. P. Shibayev, H. Lin, S. Jia, and M. Z. Hasan, *Science* **349**, 613, (2015).
- [9] Z. K. Liu, J. Jiang, B. Zhou, Z. J. Wang, Y. Zhang, H. M. Weng, D. Prabhakaran, S. K. Mo, H. Peng, P. Dudin, T. Kim, M. Hoesch, Z. Fang, X. Dai, Z. X. Shen, D. L. Feng, Z. Hussain, and Y. L. Chen, *Nat. Mater.* **13**, 677, (2014).
- [10] G. Bian, T.-R. Chang, R. Sankar, S.-Y. Xu, H. Zheng, T. Neupert, C.-K. Chiu, S.-M. Huang, G. Chang, I. Belopolski, D. S. Sanchez, M. Neupane, N. Alidoust, C. Liu, B. Wang, C.-C. Lee, H.-T. Jeng, C. Zhang, Z. Yuan, S. Jia, A. Bansil, F. Chou, H. Lin, and M. Z. Hasan, **7**, 10556, (2016).
- [11] Z. K. Liu, B. Zhou, Y. Zhang, Z. J. Wang, H. M. Weng, D. Prabhakaran, S. K. Mo, Z. X. Shen, Z. Fang, X. Dai, Z. Hussain, and Y. L. Chen, *Science* **343**, 864, (2014).
- [12] S.-Y. Xu, C. Liu, S. K. Kushwaha, R. Sankar, J. W. Krizan, I. Belopolski, M. Neupane, G. Bian, N. Alidoust, T.-R. Chang, H.-T. Jeng, C.-Y. Huang, W.-F. Tsai, H. Lin, P. P. Shibayev, F.-C. Chou, R. J. Cava, and M. Z. Hasan, *Science* **347**, 294, (2015).
- [13] M. Neupane, S.-Y. Xu, R. Sankar, N. Alidoust, G. Bian, C. Liu, I. Belopolski, T.-R. Chang, H.-T. Jeng, H. Lin, A. Bansil, F. Chou, and M. Z. Hasan, **5**, 3786, (2014).
- [14] B. Q. Lv, H. M. Weng, B. B. Fu, X. P. Wang, H. Miao, J. Ma, P. Richard, X. C. Huang, L. X. Zhao, G. F. Chen, Z. Fang, X. Dai, T. Qian, and H. Ding, *Phys. Rev. X* **5**, 031013, (2015).
- [15] Z. K. Liu, L. X. Yang, Y. Sun, T. Zhang, H. Peng, H. F. Yang, C. Chen, Y. Zhang, Y. F. Guo, D. Prabhakaran, M. Schmidt, Z. Hussain, S. K. Mo, C. Felser, B. Yan, and Y. L. Chen, *Nat. Mater.* **15**, 27, (2016).
- [16] R. Yu, H. Weng, Z. Fang, X. Dai, and X. Hu, *Phys. Rev. Lett.* **115**, 036807, (2015).
- [17] Y. Kim, B. J. Wieder, C. L. Kane, and A. M. Rappe, *Phys. Rev. Lett.* **115**, 036806, (2015).
- [18] M. Zeng, C. Fang, G. Chang, Y.-A. Chen, T. Hsieh, A. Bansil, H. Lin, and L. Fu, *arXiv:1504.03492*, (2015).
- [19] J. Nayak, S.-C. Wu, N. Kumar, C. Shekhar, S. Singh, J. Fink, E. E. D. Rienks, G. H. Fecher, S. S. P. Parkin, B. Yan, and C. Felser, **8**, 13942, (2017).
- [20] A. Yamakage, Y. Yamakawa, Y. Tanaka, and Y. Okamoto, *J. Phys. Soc. Jpn.* **85**, 013708, (2015).
- [21] G. Kresse, and J. Furthmüller, *Computational Materials Science* **6**, 15, (1996).
- [22] G. Kresse, and J. Furthmüller, *Phys. Rev. B* **54**, 11169, (1996).
- [23] J. P. Perdew, K. Burke, and M. Ernzerhof, *Phys. Rev. Lett.* **77**, 3865, (1996).
- [24] A. A. Mostofi, J. R. Yates, Y.-S. Lee, I. Souza, D. Vanderbilt, and N. Marzari, *Computer Physics Communications* **178**, 685, (2008).
- [25] A. A. Soluyanov, and D. Vanderbilt, *Phys. Rev. B* **83**, 235401, (2011).
- [26] R. Yu, X. L. Qi, A. Bernevig, Z. Fang, and X. Dai, *Phys. Rev. B* **84**, 075119, (2011).

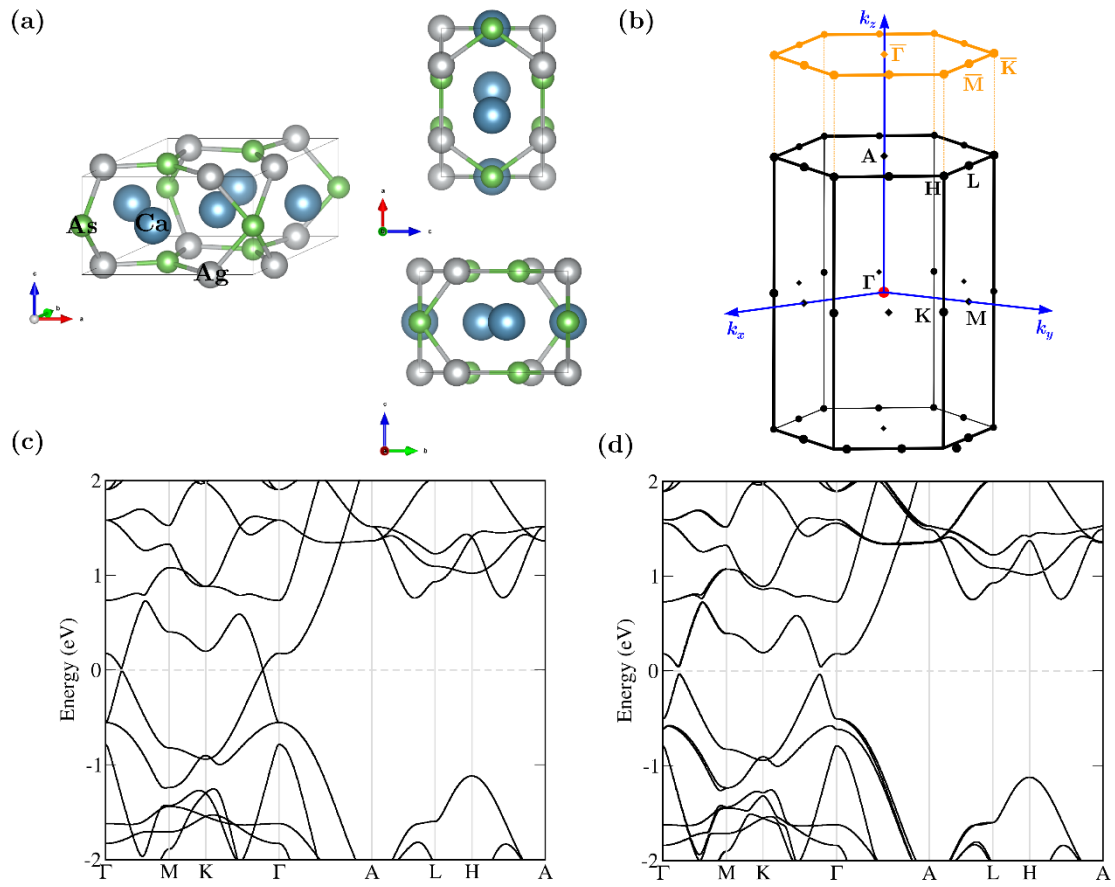


Fig.1: Crystal structure and band structure. (a) Hexagonal crystal structure of CaAgAs, (b) Bulk and (0001) projected surface Brillouin zone. Calculated bulk band structure of CaAgAs without (c) and with SOC (d).

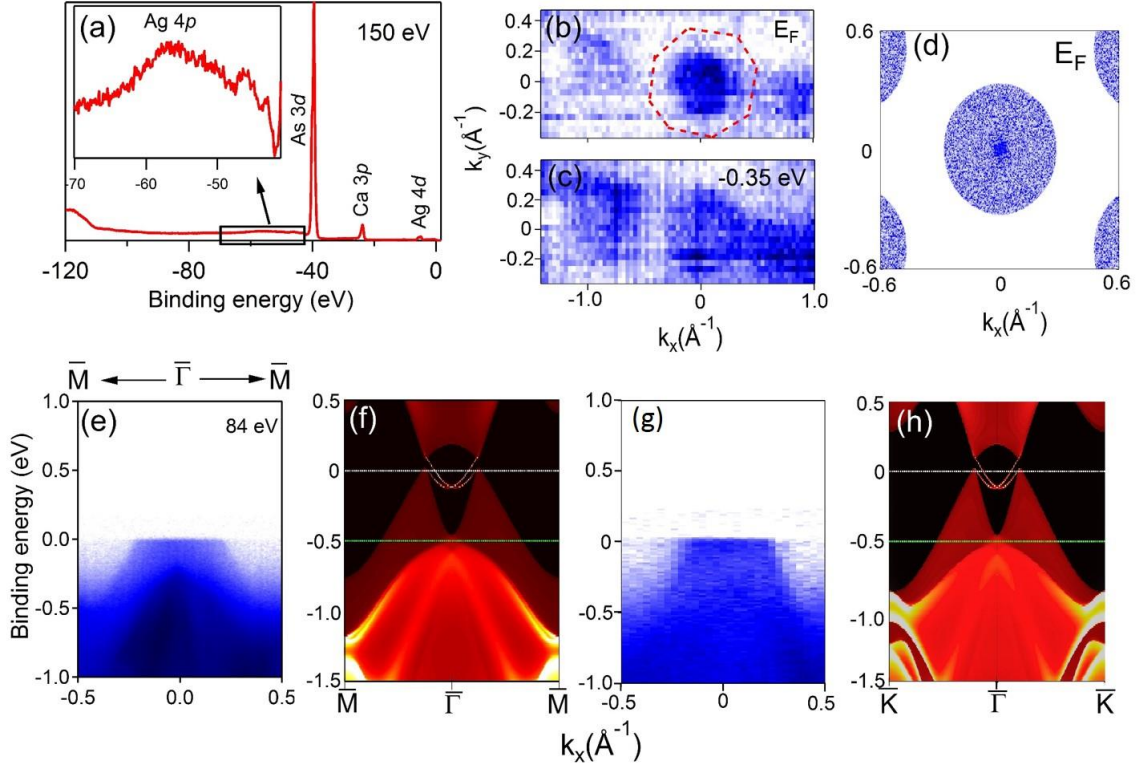


Fig.2: ARPES measurement of CaAgAs (0001) surface. (a) corelevel spectrum of CaAgAs acquired with 150 eV excitation energy showing Ca 3*p*, Ag 4*d* and As 3*d* peaks and the inset shows Ag 4*p* peak in the expanded scale. (b) Fermi surface of CaAgAs measured with 85 eV photon energy, (c) constant energy surface of CaAgAs at 0.4 eV binding energy, (d) theoretically calculated Fermi surface (e) ARPES spectra and (f) theoretically calculated spectra along $\bar{M} - \bar{\Gamma} - \bar{M}$ direction respectively, (g) and (h) similar results as (e) and (f) but measured long $\bar{K} - \bar{\Gamma} - \bar{K}$ direction.

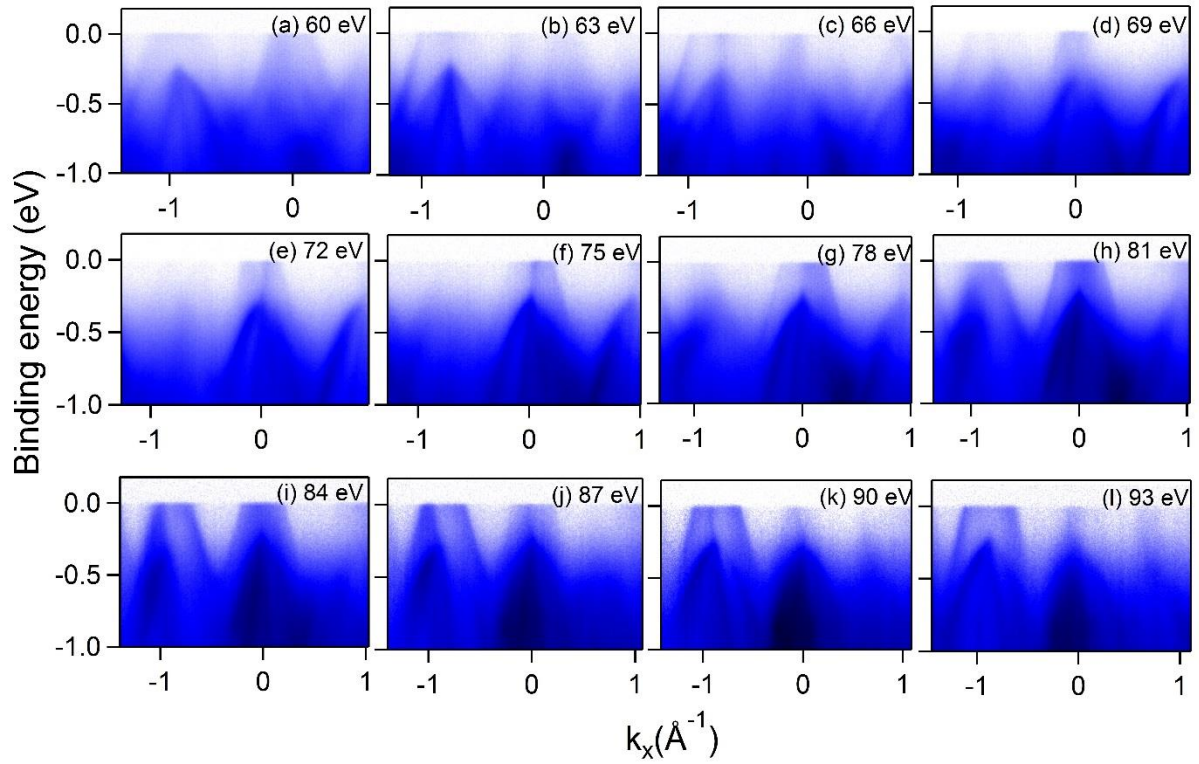


Fig. 3: Photon energy dependent ARPES measurement of CaAgAs. (a-g) ARPES spectra measured along $\bar{M} - \bar{\Gamma} - \bar{M}$ direction with photon energies between 60 eV to 93 eV at a step size of 3 eV.

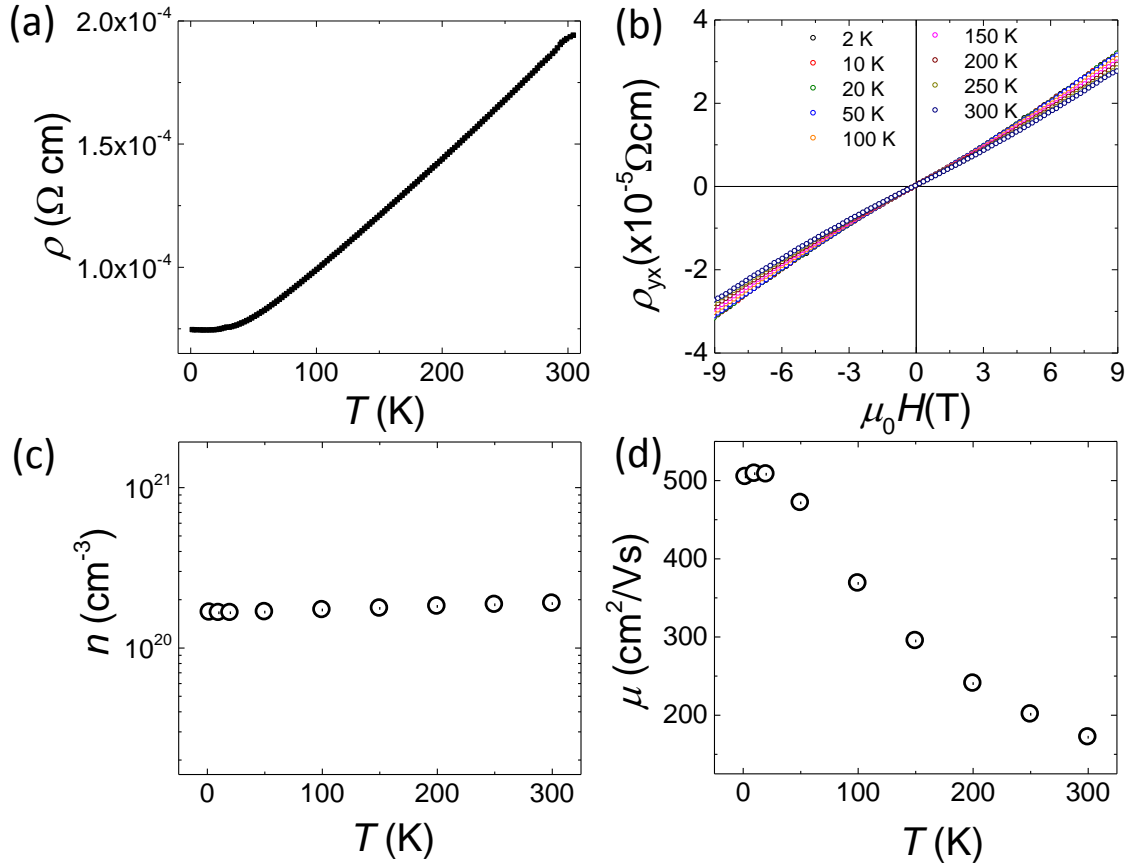


Fig. 4: Transport properties of CaAgAs. (a) $\rho(T)$ data at zero magnetic field. (b) Field dependent Hall resistivity at different temperatures. (c) and (d) show carrier concentration and mobility, respectively extracted from the Hall resistivity.